CROSS-TRACK THREE APERTURES MILLIMETER WAVE SAR SIDE-LOOKING THREE-DIMENSIONAL IMAGING[1]

Teng Xiumin[*,**] Li Daojing[*] Li Liechen[*,**] Liu Bo[*,**] Pan Zhouhao[*,**]

[*](*Science and Technology on Microwave Imaging Laboratory, Institute of Electronics, Chinese Academy of Sciences, Beijing 100190, China*)

[**](*Graduate University of Chinese Academy of Sciences, Beijing 100049, China*)

Abstract The airborne cross-track three apertures MilliMeter Wave (MMW) Synthetic Aperture Radar (SAR) side-looking three-Dimensional (3D) imaging is investigated in this paper. Three apertures are distributed along the cross-track direction, and three virtual phase centers will be obtained through one-input and three-output. These three virtual phase centers form a sparse array which can be used to obtain the cross-track resolution. Because the cross-track array is short, the cross-track resolution is low. When the system works in side-looking mode, the cross-track resolution and height resolution will be coupling, and the low cross-track resolution will partly be transformed into the height uncertainty. The beam pattern of the real aperture is used as a weight to improve the Peak to SideLobe Ratio (PSLR) and Integrated SideLobe Ratio (ISLR) of the cross-track sparse array. In order to suppress the high cross-track sidelobes, a weighting preprocessing method is proposed. The 3D images of a point target and a simulation scene are achieved to verify the feasibility of the proposed method. And the imaging result of the real data obtained by the cross-track three-baseline MMW InSAR prototype is presented as a beneficial attempt.

Key words Synthetic Aperture Radar (SAR); Sparse array; Side-looking imaging; Three-Dimensional (3D) imaging

CLC index TN957

DOI 10.1007/s11767-012-0897-5

I. Introduction

The three-Dimensional (3D) imaging Synthetic Aperture Radar (SAR) system can be used to image the observation scene in three dimensions. So it has a great potential in various applications, such as city mapping and investigation in the battlefield.

In 1999, Gierull proposed a high-resolution Airborne Downward-looking Imaging Radar (ADIR) system which combines the concepts of real and synthetic aperture[1]. In 2004, a 3D-SAR concept for a MilliMeter Wave (MMW) imaging radar was proposed in the European Radar Conference[2]. To focus along three dimensions: cross-track, along-track, and range directions respectively, a linear array combined with the SAR technique and the Linear Frequency-Modulated (LFM) pulses are employed. In 2006, a new radar system called Airborne Radar for Three-dimensional Imaging and Nadir Observation (ARTINO) was developed by FGAN-FHR[3]. A sparse array was distributed along the wings of the plane with transmitting elements at the tips and receiving elements over the remainder space. A virtually fully filled array could be obtained to achieve the cross-track resolution. In Ref. [4], by the multiple phase center aperture synthesis principle[5], an optimal sparse array obtained by simulated annealing algorithm[6] was coincident with a fully filled array, which was used to achieve the 3D imaging of the direct overflown scene.

In above studies, a fully filled array should be obtained in the cross-track direction. In this paper, based on the airborne cross-track three-baseline MMW InSAR prototype developed by Institute of Electronics, Chinese Academy of Sciences

[1] Manuscript received date: May 29, 2012; revised date: July 8, 2012.
Supported by the National Basic Research Program (973) of China (No. 2009CB72400).
Communication author: Teng Xiumin, born in 1987, female, Master Degree candidate. Science and Technology on Microwave Imaging Laboratory, Institute of Electronics, Chinese Academy of Sciences, Beijing 100190, China.
Email: xmteng@163.com.

(IECAS)[7], a sparse array formed of three virtual phase centers is used to achieve 3D image of the observation scene when the system works in side-looking mode.

II. System Description

1. Geometrical model

In the airborne cross-track three-baseline MMW InSAR prototype system, three apertures are hung at the bottom of the platform. The system installation view is shown in Fig. 1.

Fig. 1 The installation view of the cross-track apertures

Fig. 2 shows the imaging geometry of the cross-track three apertures side-looking SAR system. In the coordinate of Fig. 2, X-axis is the along-track direction, Y-axis is the cross-track direction, and Z-axis is the height direction. The platform is supposed to fly at the altitude H with the velocity v. The system works in side-looking mode, and the cross-track beam incidence angle is θ.

The three apertures are distributed along the cross-track direction to achieve the cross-track resolution. The platform flies along the along-track direction, a synthetic aperture is formed to obtain the along-track resolution. The range resolution is resulted from the broadband LFM signal, and the height resolution can be achieved by the projection of the range resolution.

2. Cross-track apertures configuration

The cross-track positions of the three apertures are shown in Fig. 3(a). A1 is the transmitting aperture, and A1, A2, A3 are the receiving apertures. Three apertures are not equispaced, the distance between two apertures are 0.6 m and 0.4 m respectively.

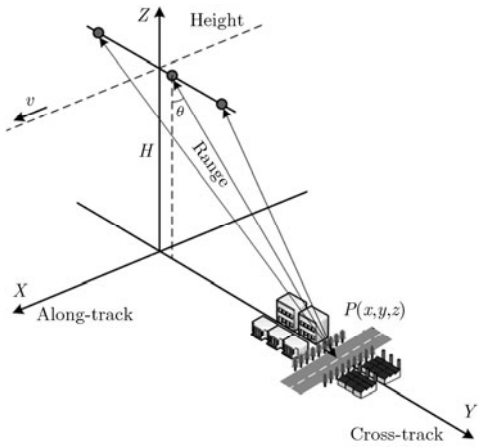

Fig. 2 The imaging geometry of the cross-track three apertures side-looking SAR system

Based on the equivalent phase center principle, a virtual phase center can be formed in the mean position of a transmitting and a receiving aperture. So three virtual phase centers can be obtained in the cross-track direction. The virtual phase centers configuration is shown in Fig. 3(b).

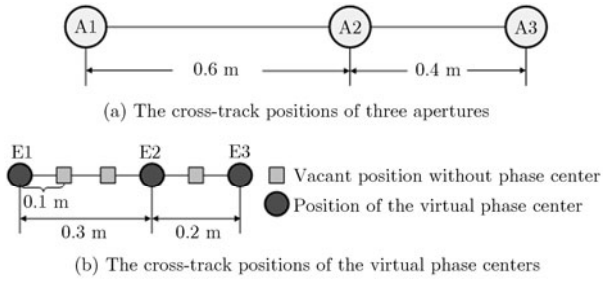

(a) The cross-track positions of three apertures

(b) The cross-track positions of the virtual phase centers

Fig. 3 The cross-track apertures configuration

These three virtual phase centers form a sparse array in the cross-track direction, so the 3D imaging can be achieved using this system.

As shown in Fig. 3(b), the cross-track three virtual phase centers occupy 6 equispaced positions with interval of 0.1 m. And the configuration of the virtual phase centers can be expressed as [1 0 0 1 0 1], whose autocorrelation function is shown in Fig. 4. It is shown that [1 0 0 1 0 1] is a random sequence.

III. Cross-track Beam Pattern Analysis

The beam pattern of the cross-track sparse array is analyzed to evaluate its PSLR and ISLR. The diameter of the cross-track aperture is 0.2 m,

the transmitting signal wavelength is 0.0086 m, so the cross-track beamwidth is about 2.46°. The cross-track beam incident angle is 35°.

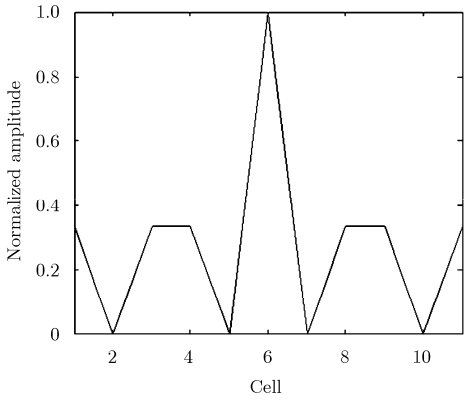

Fig. 4 The autocorrelation function of [1 0 0 1 0 1]

The beam pattern of the 0.2 m real aperture will be used as a weight to control the PSLR and ISLR of the cross-track sparse array[8]. Because the cross-track beam incident angle is 35°, the normal direction beam pattern of the 0.2 m real aperture should be right shifted 35° to match with the cross-track sparse array, as shown in Fig. 5(a). The 0.2 m real aperture could be formed of 46 antenna elements with a distance of a half wavelength. The beam pattern of the cross-track sparse array is shown in Fig. 5(b).

The combined beam pattern is obtained by multiplying the sparse array beam pattern and the 0.2 m real aperture beam pattern, as illustrated in Fig. 5(c). And Fig. 5(d) shows the part of Fig. 5(c) in the mainlobe range (from 32.54° to 37.46°) of the 0.2 m real aperture beam pattern. In Fig. 5(c) the ISLR is about –5.40 dB (the integrated range is from –90° to –90°), and in Fig. 5(d) it is about –8.40 dB (the integrated range is from 32.54° to 37.46°). As shown in Fig. 5(d), the PSLR of the combined beam pattern is –10.66 dB.

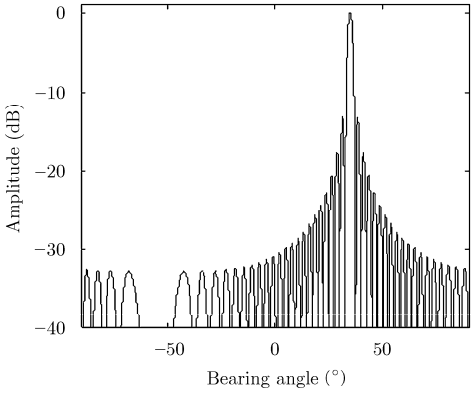

(a) Beam pattern of the 0.2 m real aperture

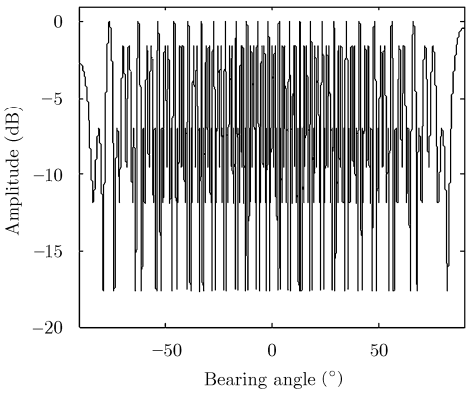

(b) Beam pattern of the cross-track sparse array

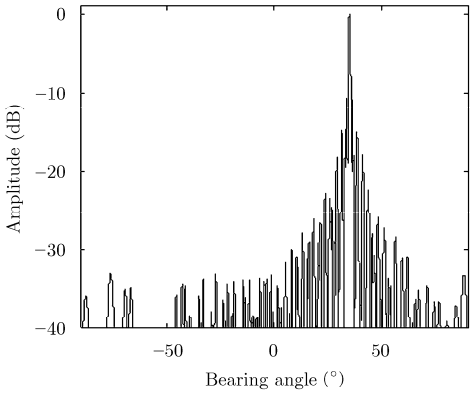

(c) The combined beam pattern

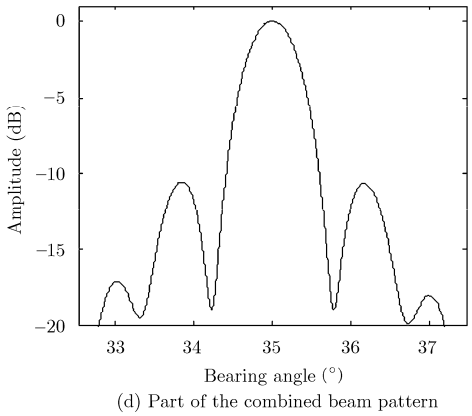

(d) Part of the combined beam pattern

Fig. 5 Cross-track beam pattern analysis results

IV. 3D Imaging Algorithm

1. Received signal

Based on the imaging geometry shown in Fig. 2, assume that the m-th along-track sampling posi-

tion is $u_m (m = 1,2,\cdots,M$, M is the number of pulse), the cross-track position of the n-th aperture is v_n $(n = 1,2,3)$. One of the cross-track apertures (v_1) is the transmitting aperture, and it transmits LFM signal, which can be expressed as

$$p(t) = \mathrm{rect}\left(\frac{t}{T_p}\right)\exp\left\{j2\pi f_0 t + j\pi K_r t^2\right\} \tag{1}$$

where t denotes the fast time, f_0 is the center frequency, T_p is the signal time width, and K_r is the chirp rate.

Consider that the i-th point target is located at $\boldsymbol{P}_i(x_i, y_i, z_i)$ with the reflectivity σ_i. So the echo signal received by the n-th cross-track aperture in the m-th along-track sampling position can be written as

$$s(t, u_m, v_n) = \sum_i \sigma_i p\left(t - \tau(u_m, v_n, \boldsymbol{P}_i)\right) \tag{2}$$

where $\tau(u_m, v_n, \boldsymbol{P}_i)$ is the time delay from the transmitting aperture v_1 to the receiving aperture v_n passing the point target $\boldsymbol{P}_i$.

$$\tau(u_m, v_n, \boldsymbol{P}_i) = \frac{R_{ti} + R_{ri}}{c} \tag{3}$$

$$\begin{cases} R_{ti} = \sqrt{(u_m - x_i)^2 + (v_1 - y_i)^2 + (H - z_i)^2} \\ R_{ri} = \sqrt{(u_m - x_i)^2 + (v_n - y_i)^2 + (H - z_i)^2} \end{cases} \tag{4}$$

where c is the speed of light, R_{ti} is the distance between the transmitting aperture v_1 and the point $\boldsymbol{P}_i$, R_{ri} is the distance between the point $\boldsymbol{P}_i$ and the receiving aperture v_n.

2. Phase compensation for the virtual phase center

Let the cross-track position of the k-th virtual phase center is v_{ek} $(k = 1,2,3)$, which is obtained by the signal transmitted by aperture v_1 and received by aperture v_k.

In order to make the phase of the echo signal received by the k-th cross-track aperture coincident with the signal transmitted and received by the virtual phase center itself, the phase of the received signal should be compensated. At the m-th along-track sampling position, the phase difference can be expressed as

$$\Delta\phi_k = \frac{2\pi}{\lambda}(R_t + R_{rk}) - \frac{4\pi}{\lambda}R_{ek} \tag{5}$$

$$\begin{cases} R_t = \sqrt{(u_m - x_0)^2 + (v_1 - y_0)^2 + (H - z_0)^2} \\ R_{rk} = \sqrt{(u_m - x_0)^2 + (v_k - y_0)^2 + (H - z_0)^2} \\ R_{ek} = \sqrt{(u_m - x_0)^2 + (v_{ek} - y_0)^2 + (H - z_0)^2} \end{cases} \tag{6}$$

where λ is the wavelength, and $\boldsymbol{P}_0(x_0, y_0, z_0)$ is the center point of the observation scene.

3. 3D wavenumber domain imaging algorithm[4]

Suppose the motion compensation processing has been finished for the echo signals. After above compensation processing, the echo signal can be approximately written as

$$s(t, u, v) = \sum_i \sigma_i p\left(t - \tau(u, v, \boldsymbol{P}_i)\right) \tag{7}$$

$$\tau = \frac{2\sqrt{(u - x_i)^2 + (v - y_i)^2 + (H - z_i)^2}}{c} \tag{8}$$

where u denotes the along-track sampling position, v denotes the cross-track sampling position. Because the cross-track sampling position is sparse, s will be filled with zeros in the vacant cross-track sampling position.

Apply 3D Fourier transform to Eq. (7), we can get the 3D wavenumber domain signal

$$S(k_t, k_u, k_v) = P(k_t) \cdot \sum_i \sigma_i \exp\left\{-j\left(\sqrt{4k_t^2 - k_u^2 - k_v^2}\, z_i - k_u x_i - k_v y_i\right)\right\} \tag{9}$$

where $k_t = 2\pi f_0 / c$ denotes the fast-time wavenumber, k_u and k_v are the along-track wavenumber and the cross-track wavenumber respectively.

Construct a matched filter using the center point of the observation scene $\boldsymbol{P}_0(x_0, y_0, z_0)$, then transform it to the three-dimensional wavenumber domain. It can be written as

$$H(k_t, k_u, k_v) = P^*(k_t) \cdot \exp\left\{j\left(\sqrt{4k_t^2 - k_u^2 - k_v^2}\, z_0 - k_u x_0 - k_v y_0\right)\right\} \tag{10}$$

The output of matched filter can be written as

$$\begin{aligned} S_M(k_t,k_u,k_v) &= S(k_t,k_u,k_v)H(k_t,k_u,k_v) \\ &= |P(k_t)|^2 \sum_i \sigma_i \\ &\cdot \exp\left\{-j\left(\sqrt{4k_t^2-k_u^2-k_v^2}(z_i-z_0)\right.\right. \\ &\left.\left.-k_u(x_i-x_0)-k_v(y_i-y_0)\right)\right\} \end{aligned} \tag{11}$$

Because k_t is not orthogonal with the k_u and k_v plane, the 3D STOLT transform is adopted to obtain an orthogonal coordinate in the three dimensional wavenumber domain. The transform expression is

$$\begin{cases} k_x = k_u \\ k_y = k_v \\ k_z = \sqrt{4k_t^2-k_u^2-k_v^2} \end{cases} \tag{12}$$

Then phase in Eq. (11) can be written as

$$\begin{aligned} \phi_i(k_x,k_y,k_z) &= k_x(x_i-x_0)+k_y(y_i-y_0) \\ &+k_z(z_i-z_0) \end{aligned} \tag{13}$$

The targets can be reconstructed through 3D inverse Fourier transform.

Because the cross-track array is sparse, the cross-track PSLR is relatively high. In order to improve the image quality, a weighting preprocessing method is proposed to suppress the cross-track sidelobes. The processing steps will be presented in the following section in detail.

V. Experimental Results

1. System parameters

The platform flies at the altitude of 1396 m with the velocity of 47.6 m/s. The lowest elevation of the observation scene is about 346 m. The system works in Ka-band, with a bandwidth of 400 MHz, a Pulse Repeat Frequency (PRF) of 4 kHz. While using the real data, the along-track data is down sampled 4 times, so the equivalent PRF is 1 kHz. The system parameters are shown in Tab. 1 in detail.

2. Simulation results

Based on the system parameters presented in Tab. 1, the side-looking 3D image of a point target (located at (0 m, 735 m, 346 m)) is achieved. The 3D image is shown in Fig. 6(a), and Fig. 6(b) is the cross-track and height plane in the along-track 0 m. The point target imaging result demonstrates that it is feasible to achieve side-looking 3D imaging using this system, while the cross-track resolution is low (the cross-track resolution of the point target is about 11 m). When the system works in side-looking mode, the cross-track resolution and the height resolution are coupling, and the low cross-track resolution is partly transformed into the height uncertainty (The phenomena is illustrated in Fig. 6(b)).

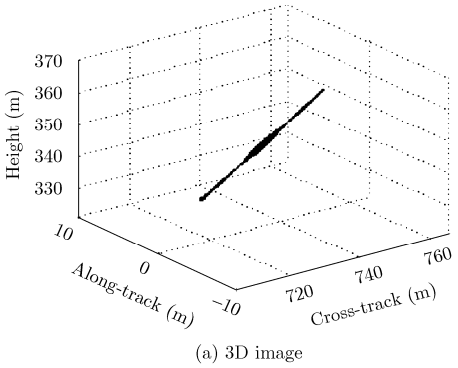

(a) 3D image

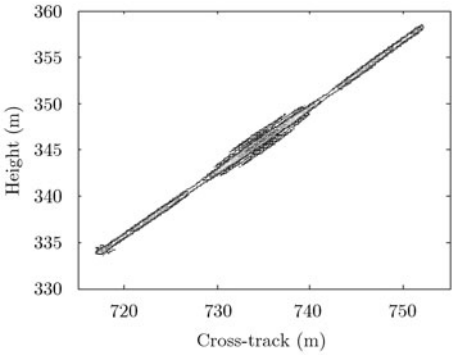

(b) The cross-track and height plane

Fig. 6 Side-looking imaging result of a point target

Because the cross-track array is sparse, the cross-track PSLR is relatively high. In order to suppress the cross-track sidelobes, a preprocessing method weighting the cross-track spectrum by a window function is proposed.

The cross-track spectrum of the sparse array is shown in Fig. 7(a). The cross-track spectrum of the fully filled array with 6 apertures is used as the reference function to construct a rectangle window. After multiplying the sparse array cross-track

spectrum and the window function, the cross-track spectrum is show in Fig. 7(b).

Tab. 1 System parameters

Parameters	Value
Center frequency	35 GHz
Bandwidth	400 MHz
Cross-track beam incident angle	35°
Length of the cross-track array	0.5 m
Distance of the sparse array	0.1 m
PRF	1000 Hz
Cross-track resolution (Range is 1280 m)	about 11 m
Platform altitude	1396 m
Carrier velocity	47.6 m/s
Number of cross-track apertures	3
Aperture diameter	0.2 m
Beam width	2.46°
Range resolution	about 0.5 m
Along-track resolution	0.5 m

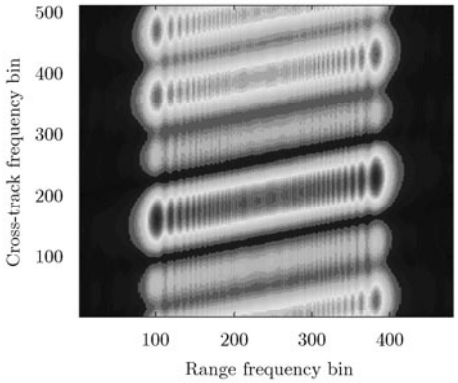

(a) Before weighting by the window function

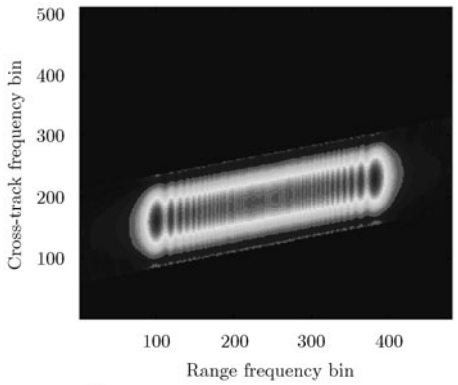

(b) After weighting by the window function

Fig. 7 Spectrum of the range and cross-track directions

Through the weighting preprocessing, the side-looking 3D image of the point target is shown

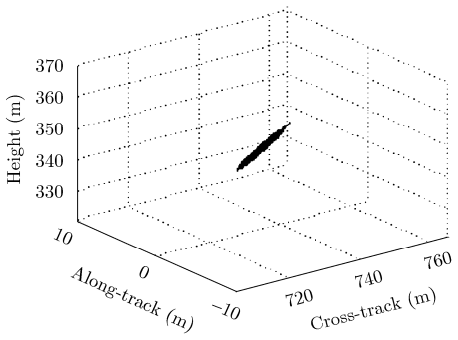

(a) 3D image

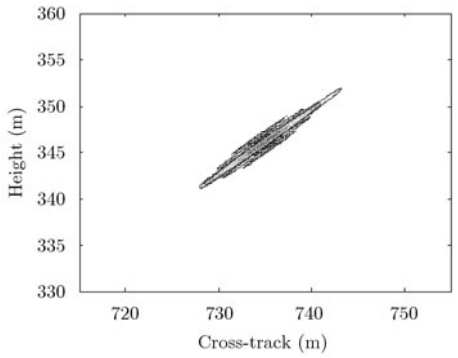

(b) The cross-track and height plane

Fig. 8 Side-looking imaging result of a point target after weighting preprocessing

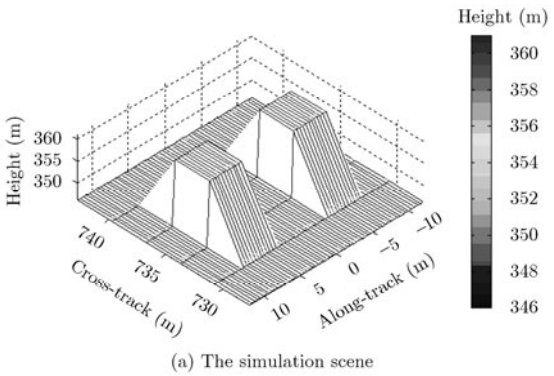

(a) The simulation scene

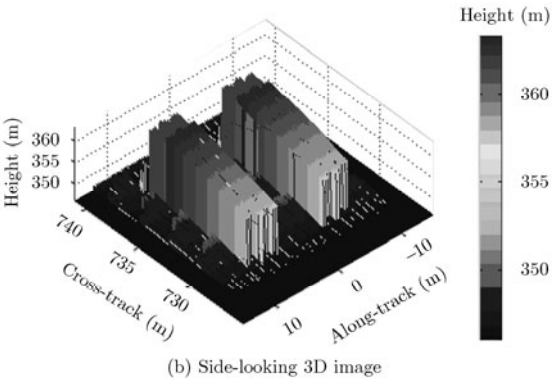

(b) Side-looking 3D image

Fig. 9 Side-looking imaging result of a simulation scene

in Fig. 8(a), and Fig. 8(b) shows the cross-track and height plane in the along-track 0 m. It is shown that the cross-track sidelobes are suppressed effectively.

Then a simulation scene is constructed, as shown in Fig. 9(a), which contains two planes with the same height (with elevation of 361 m). The side-looking 3D image is achieved using the imaging algorithm introduced in this paper. Fig. 9(b) shows the imaging result, the two planes can be distinguished.

3. Side-looking 3D imaging result using the real data

Using the imaging algorithm presented above, the real data obtained by the cross-track three-baseline millimeter wave InSAR prototype developed by IECAS is used to achieve 3D imaging of the observation scene. The system parameters are presented in Tab. 1. Fig. 10(b) shows the 3D imaging result, the 2D image (the part contained in the two red lines) is shown in Fig. 10(a) as the references. In the imaging area, there are three trees with the height about 15–25 m. The size of the 3D image shown in Fig. 10(b) is about 48 m × 25 m × 40 m (along-track × cross-track × height).

VI. Conclusion

Based on the cross-track three apertures millimeter wave SAR system, three virtual phase centers are obtained through one-input and three-output. And a sparse array is formed in the cross-track direction by the three virtual phase centers, which can be used to achieve the cross-track resolution. The cross-track resolution is low because of the short sparse array. When the system works in side-looking mode, the cross-track resolution and the height resolution will be coupling, so the low cross-track resolution will partly be transformed into the height uncertainty. The beam pattern of real aperture is used as a weight to improve the PSLR and ISLR of the sparse array. In order to improve the imaging quality, a weighting preprocessing method is proposed to suppress the high cross-track sidelobles. The simulation results indicate that the method proposed in this paper is feasible. Finally, we attempt to achieve the side-looking 3D image of the real scene using the real data obtained by the airborne cross-track three-baseline MMW InSAR prototype developed by IECAS.

This work would be an important guidance for developing millimeter wave 3D SAR in the future.

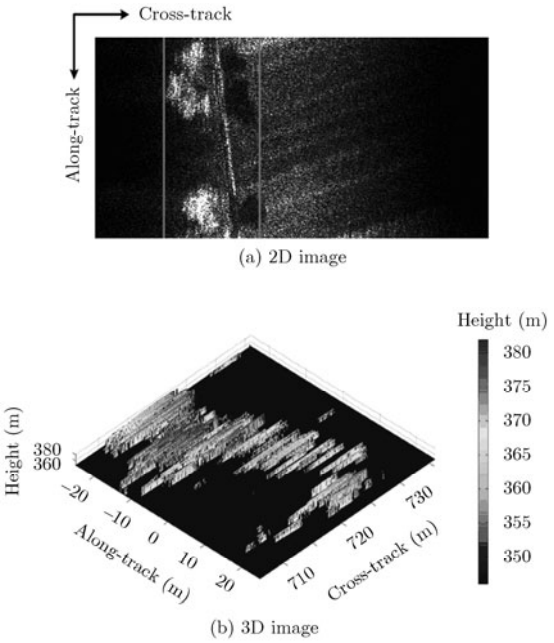

Fig. 10 Side-looking imaging result of the real data

References

[1] C. H. Gierull. On a concept for an airborne downward-looking imaging radar. *International Journal of Electronics and Communications* (*AEÜ*), **53**(1999)6, 295–304.

[2] R. Giret, H. Jeuland, and P. Enert. A study of 3D-SAR concept for a millimeter wave imaging radar onboard an UAV. European Radar Conference 2004, Amsterdam, Netherland, October 14–15, 2004, 201–204.

[3] J. Klare, A. R. Brenner, and J. H. G. Ender. A new airborne radar for 3D imaging–image formation using the ARTINO principle. 6th European Conference on Synthetic Aperture Radar (EUSAR 2006), Dresden, Germany, May 16–18, 2006.

[4] Hou Yingni, Li Daojing, and Hong Wen. The thinned array time division multiple phase center aperture synthesis and application. 2008 IEEE International Geoscience and Remote Sensing Symposium (IGARSS 2008), Boston, MA, USA, July 7–11, 2008, 25–28.

[5] Li Zhenfang, Bao Zheng, Wang Hongyang, *et al.*. Performance improvement for constellation SAR using signal processing techniques. *IEEE Transactions on Aerospace and Electronic Systems*, **42**(2006)2, 436–452.

[6] C. S. Ruf. Numerical annealing of low-redundancy linear arrays. *IEEE Transactions on Antennas and Propagation*, **45**(1993)1, 85–90.

[7] Li Daojing, Liu Bo, Pan Zhouhao, *et al.*. Airborne MMW InSAR interferometry with cross-track three-baseline antennas. 9th European Conference on Synthetic Aperture Radar (EUSAR 2012), Nuremberg, Germany, April 23–26, 2012, 301–303.

[8] Li Daojing, Hou Yingni, and Hong Wen. The sparse array aperture synthesis with space constraint. 8th European Conference on Synthetic Aperture Radar (EUSAR 2010), Dresden, Germany, June 7–10, 2010, 950–953.